https://doi.org/10.48047/AFJBS.6.Si4.2024.4757-4771

African Journal of Biological Sciences

Journal homepage: http://www.afjbs.com

Research Paper Open Access

Synthesis and characterization of aWFS- Fe_3O_4composite for a photodegradation Study

Chandrashekhar R. Patil[1], Aishwarya S Nikam[2], Dnyandev N. Zambare[3]*

[1,3*]Department of Chemistry, Kisan Veer Mahavidyalaya, Wai, Satara-412803, Maharashtra, India,[2]School of Nanoscience, Shivaji University, Kolhapur-416004, Maharashtra, India

***Corresponding author:** Dnyandev N. Zambare
*Email:dnzambare123@gmail.com

Article History
Volume 6, Issue Si4, 2024
Received: 1 July 2024
Accepted: 20 July 2024
Doi:
10.48047/AFJBS.6.Si4.2024.4757-4771

Abstract
The photodegradation technique has been identified as the most effective environmentally friendly approach for removing organic dyes from contaminated water. In this study, waste foundry sand- ferrite (WFS-Fe_3O_4) composites were synthesized using co-precipitation method.The composite was characterized by X-ray diffraction (XRD), Raman spectroscopy, scanning electron microscopy (SEM), Fourier transform infrared spectroscopy (FT-IR), zeta potential, and particle size analysis. FT-IR confirmed the presence of strong chemical bonding and functional groups at the interface of WFS and Fe_3O_4. The photocatalytic activity of these catalysts was assessed through the degradation of methylene blue (MB) dye under visible light irradiation. The results demonstrate that the synthesized composites exhibit significant magnetic and photocatalytic performance.

Keywords- WFS-Fe_3O_4 composite, Co-Precipitation, Photodegradation study, Waste management,

1.Introduction

Our environment is impacted by numerous hazardous human activities, making the elimination of harmful materials and pollutants an urgent necessity for mitigating human pollution in the twenty-first century [1, 2]. This involves transforming harmful substances into safer, less polluting forms. Semiconductor nanoparticles are an important class of self-cleaning photocatalysts, utilized to degrade harmful dyes in wastewater [3, 4]. Recent studies have leveraged photocatalysis to decompose carcinogenic and aromatic residues into less harmful byproducts [5, 6].

A clean environment is essential for sustaining life on Earth and promoting health, providing critical resources such as food, air, and water for all living organisms [7, 8]. Therefore, it is crucial

for everyone to contribute to protecting the environment from various pollutants [9, 10]. Organic pollutants and hazardous chemicals from the chemical, agricultural, culinary, and textile industries pose constant threats to water and air, essential resources for life [11, 12]. These compounds can be toxic and carcinogenic, obstructing sunlight penetration in water bodies, thus hindering photosynthesis and harming aquatic life [13, 14]. Dyes also pose public health risks by accumulating in living organisms, leading to organ damage [15, 16]. Azo dyes, extensively used in the food, cosmetic, and pharmaceutical industries, are the most studied commercial organic dyes due to their high toxicity and prevalence in the textile industry, comprising 70% of the dyes used [17]. The removal of these pollutants through environmentally safe and effective methods is crucial.

The scientific community has proposed various wastewater treatment techniques, such as solvent extraction, ultrafiltration, evaporation, and reverse osmosis [18]. However, these methods remove contaminants from water without converting them into harmless byproducts [19]. The detrimental effects of pathogens and wastewater contamination on humans, crops, and animals have made wastewater treatment increasingly important. Effective wastewater treatment at both personal and governmental levels is necessary to protect the environment from pollution [20]. Traditional technologies like chemical oxidation, membrane filtration, biological degradation, and plasma ozonization have been insufficient due to inefficiency, complexity, lengthy processes, disposal issues, and economic non-viability [21, 22].

Solar energy is often considered the most effective, accessible, and sustainable energy source on Earth. Visible light accounts for 43% of the sun spectrum's energy, while the UV region contributes only 4% [23]. For photocatalysis to efficiently utilize solar energy, designing effective photocatalysts sensitive to visible light is essential [24]. The general mechanism of photocatalysis involves the formation of active electron-hole pairs in a semiconductor's valence band, which are then transferred to the conduction band in the presence of light energy [25, 26]. These charged species facilitate species adsorption and generate superoxide and hydroxide radicals, which participate in oxidation-reduction degradation processes, making them vital in photocatalysis [27].

Our research aims to remove pollutants from contaminated water in an environmentally friendly manner. We focused on removing a model azo dye pollutant from polluted water using a synthesized WFS-Fe_3O_4 catalyst. The photocatalytic activity of the catalyst was investigated by optimizing essential reaction parameters, such as concentration, solution pH, anddye concentration, for improved pollutant degradation.

2. Materials and methods

In this study, reagent-grade compounds were used without further purification. The following materials were employed: Waste Foundry Sand (WFS): Collected near Kolhapur, Maharashtra, India. Ferric Nitrate [$Fe(NO_3)_3 \cdot 9H_2O$] 98% purity. Sodium Hydroxide (NaOH): 97% purity.

2.1. Synthesis of WFS-Fe_3O_4 by co-precipitation method

Initially, 3 g of Waste Foundry Sand (WFS) was combined with 25 ml of distilled water containing dissolved ferric nitrate. The mixture was stirred for 1 hour at room temperature while 10 ml of sodium hydroxide (NaOH) was added dropwise until the pH reached 10. The resulting product was then washed and centrifuged, followed by calcination at 400 °C for 2 hours to enhance interaction.

2.2. Characterization

The prepared sample was characterized using various techniques. The morphology was examined by scanning electron microscopy (SEM) with JEM-2100 200 kV (Japan) and TESCAN MIRA3 XM (Czech Republic) devices. The crystal structure and phase identification were investigated by X-ray diffraction (XRD) analysis using a Bruker D2-Phaser X-ray diffractometer. Fourier transform infrared (FT-IR) spectra were recorded on a JASCO FT-IR 4600 type A (Sr. no. D044761786) in the range of 400−4000 cm^{-1}. The vibrational properties were studied using a Confocal Raman Microscope System (Model: INCIA0120-20, Make: Renishaw). The photodegradation percentage of methylene blue (MB) was determined using an ultraviolet-visible (UV-Vis) spectrophotometer (EQIP-TRONICS, Digital Spectrophotometer, EQ 825) at λ_max = 664 nm, with a wavelength range of 400 to 800 nm. Zeta potentials of the magnetic ferrite nanoparticles were measured in aqueous dispersion based on their electrophoretic mobility.

2.3. Photocatalysis experiments.

The photocatalytic performance of the synthesized WFS-Fe_3O_4 was evaluated through the degradation of methylene blue (MB) and methyl red under sunlight. The photocatalytic experiments were conducted between 9:30 a.m. and 2:30 p.m. on weekdays. A 100-mL solution of MB (25 mg/L) was prepared in distilled water and stirred magnetically for 20 minutes. This solution was then treated with 50 mg of the synthesized catalyst. To achieve adsorption-desorption equilibrium between the photocatalyst and dye solution, the suspensions were stirred continuously and kept in a dark chamber for 30 minutes before exposure to sunlight. Subsequently, the solution was exposed to sunlight, and samples were extracted at regular intervals. The initial pH of the solution (approximately 7) was adjusted to a suitable level using 0.1 M NaOH and 0.1 M HCl as needed. The photodegradation efficiency of MB was calculated using the following equation:

Photodegradation efficiency (%) $= \left(\frac{C0 - Ct}{C0} \right) \times 100\ \% = \left(\frac{A0 - A\,t}{A0} \right) \times 100\%$

Where, C_0 is the initial concentration of MB, Ct is the concentration of MB at time t, $A_0$is the initial absorbance of MB, and At is the absorbance at time t, in accordance with the Beer-Lambert Law.

3. Result and discussion

3.1XRD analysis

Figure.2, illustrates the successful synthesis of a composite sorbent consisting of waste foundry sand (WFS) and Fe_3O_4, confirmed by X-ray diffraction (XRD) analysis. The presence of Fe (II) oxide was also detected in the WFS-Fe_3O_4 composite. Characteristic peaks corresponding to silicon (Si) were identified at 2θ values of 18.3° (111), 23.7° (210), and 26.1° (211), while peaks characteristic of Fe_3O_4 were observed at 35.6° (311) and 43.2° (400). These diffraction peaks are consistent with the WFS-Fe_3O_4 composite, as referenced in the PDF 00-039-1346 standard [28, 29].

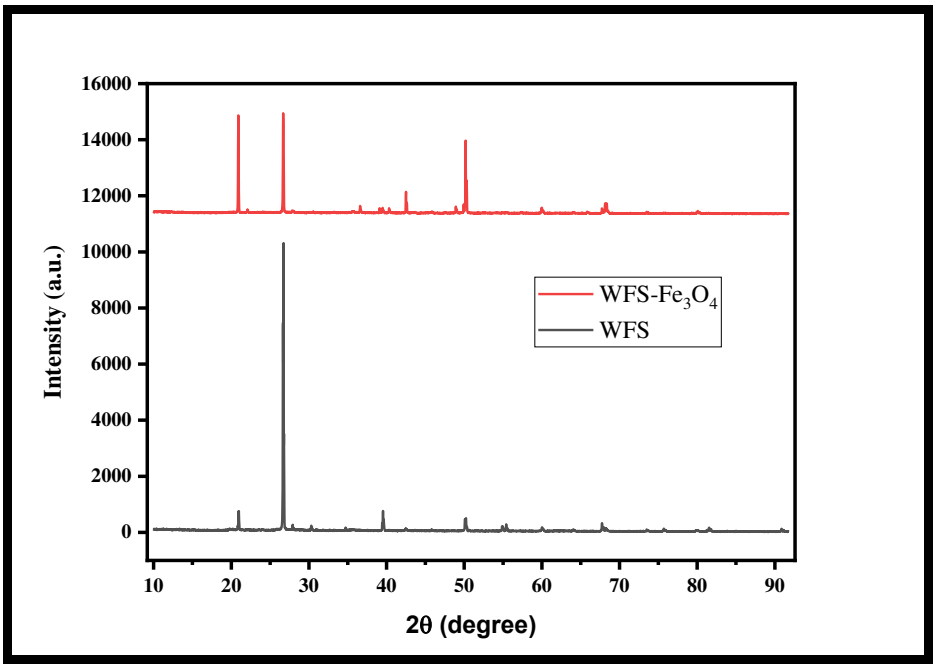

Figure 2. X-ray diffraction pattern of WFS-Fe_3O_4 and WFS

3.2. FT-IR analysis

Figure.3,represents the Fourier-transform infrared (FTIR) spectrum of the WFS-Fe_3O_4 composite, recorded over the spectral range of 400 to 4000 cm^{-1}. This analysis reveals several characteristic vibrational bands that provide insights into the functional groups and bonding interactions within the composite material.The broad bands observed at approximately 3200 cm^{-1} and 3500 cm^{-1} are indicative of the presence of adsorbed water molecules and hydroxyl (OH) functional groups [30]. These bands are typically associated with the stretching vibrations of O-H bonds, suggesting that the composite material contains moisture and hydroxyl groups, which can be attributed to surface interactions or intrinsic hydroxyl content within the material. A distinct band at 1619 cm^{-1} corresponds to the Fe-O-H stretching vibrations. This band signifies the interaction between iron and hydroxyl groups, further confirming the presence of hydroxyl functionalities within the composite structure. The Fe-O-H stretching is a critical marker for identifying hydroxylated metal oxides, which play a vital role in the material's chemical behavior and reactivity. Additionally, the absorption peak in the region between 400 and 600 cm^{-1} is characteristic of Fe-O ion oscillations [31-33]. This range is typically associated with the stretching vibrations of Fe-O bonds in various phases of iron oxide. The presence of these peaks indicates the formation of iron oxide (Fe_3O_4) within the composite, as these vibrational modes are specific to the lattice vibrations of iron oxide structures.

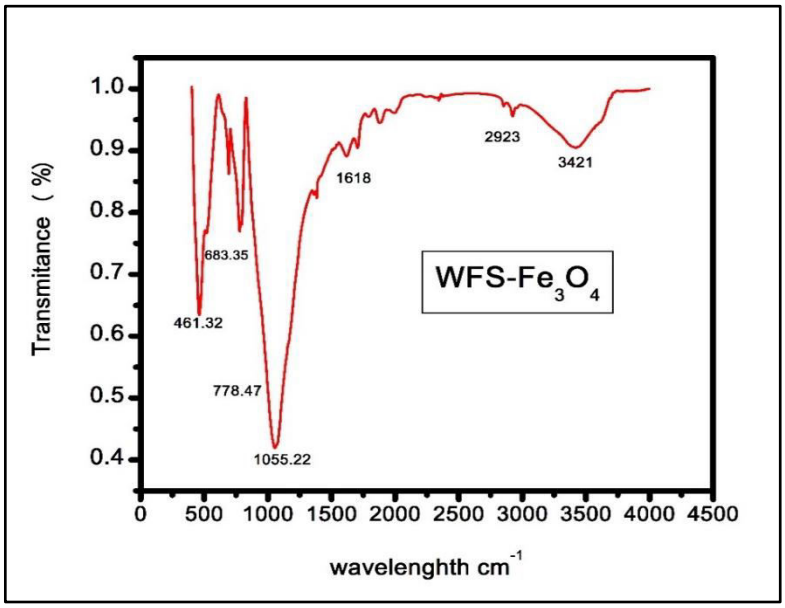

Figure.3. FTIR spectrum of WFS- Fe_3O_4.

3.3. Raman analysis

The Raman spectroscopy analysis provides critical insights into the structural and compositional characteristics of the WFS-Fe_3O_4 composite. The Raman spectrum reveals several distinctive peaks that are indicative of the material's phase and molecular interactions. The observed Raman peaks at 228 cm^{-1}, 401 cm^{-1}, and 482 cm^{-1} are characteristic of the WFS-Fe_3O_4 composite [37, 38]. These peaks correspond to the vibrational modes specific to iron oxide within the waste foundry sand (WFS) matrix. These particular peaks are signatures of the Fe_3O_4 phase, confirming its presence in the composite material. WFS ferrites, including WFS-Fe_3O_4, are known to exhibit an inverted spinel-type crystal structure. This structure influences the Raman spectral features, particularly in the range of 600-730 cm^{-1}. Within this range, the main Raman feature is composed of two distinct bands associated with the stretching vibrations of the tetrahedral cages in the spinel lattice. One of these bands, occurring at lower energies around 660 cm^{-1}, is attributed to the Fe-O bonds [34-38]. The presence of this band is a clear indication of the Fe_3O_4 phase, as the Fe-O stretching vibrations are characteristic of this iron oxide's tetrahedral sites. These bands reflect the internal lattice dynamics and confirm the structural integrity of the Fe_3O_4 within the WFS matrix. The Raman peaks and their corresponding assignments are consistent with previous studies and literature references, providing a reliable verification of the composite's composition. The distinct vibrational modes observed in the Raman spectrum are crucial for understanding the bonding environment and the crystallographic nature of the synthesized composite.

−1

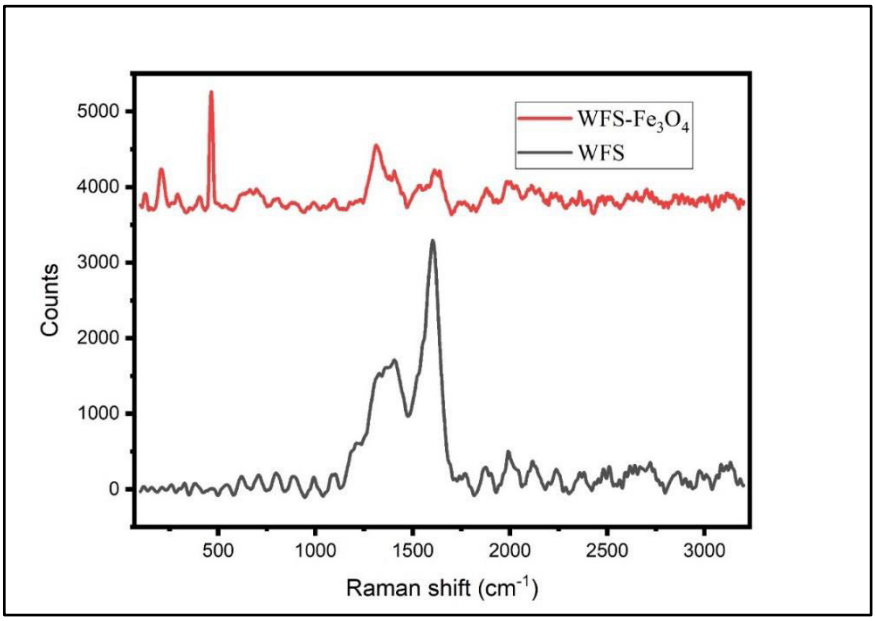

Figure.4. Raman spectrum of WFS-$Fe_3O_4$and WFS.

3.4. SEM analysis

The field emission scanning electron microscopy (SEM) images captured in Figure 5 (c, d) provide valuable insights into the microstructure and morphology of the synthesized composite material, highlighting its surface features and particle distribution.

The observed micrographs reveal that the structure exhibits rough surfaces, sharp corners, and a compact regular pore structure. This morphology is characteristic of the waste foundry sand (WFS) substrate, which possesses a high surface area and a unique structure conducive to the deposition of materials such as Fe_3O_4. The irregular surface morphology and well-defined pore structure of WFS provide sample sites for anchoring and immobilizing Fe_3O_4 nanoparticles [39, 40].

Upon closer examination, it is evident that the magnetic iron particles are evenly distributed across the surface of the WFS substrate. This uniform distribution indicates successful integration of the Fe_3O_4 particles onto the WFS matrix, leading to a homogeneous composite material with magnetic properties. This distribution is essential for ensuring effective utilization of the magnetic properties of Fe_3O_4 in applications such as magnetic separation and targeted drug delivery.

The SEM images also provide a closer look at the morphology of the Fe_3O_4 particles themselves. The images depict Fe_3O_4 particles with semi-spherical shapes, exhibiting virtually uniform distribution on the WFS substrate. However, some agglomeration of particles is also observed, indicating potential interactions and bonding between neighboring Fe_3O_4 particles. This agglomeration phenomenon can influence the material's properties and behavior, particularly in terms of its magnetic and catalytic activities [41, 42].

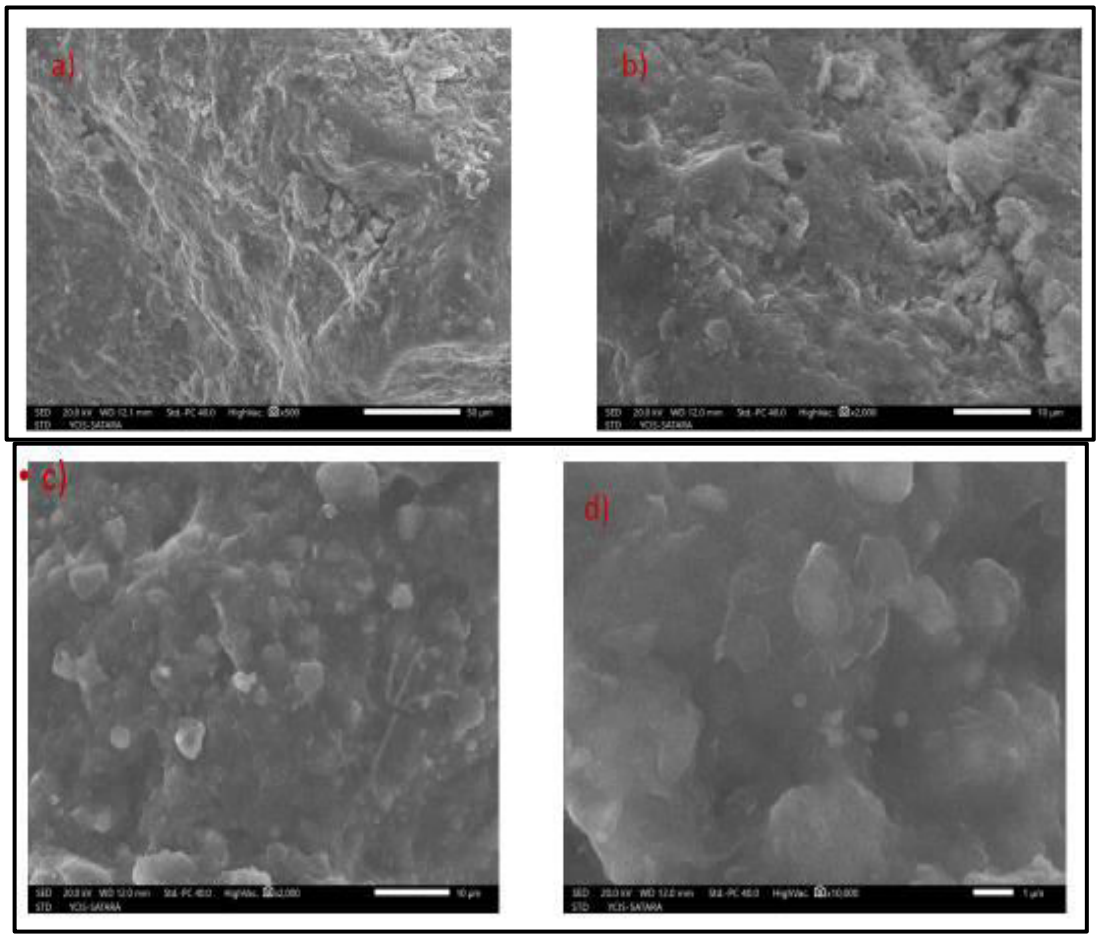

Figure.5.SEM images of(a, b)WFS and (c, d) WFS-Fe_3O_4

3.6. Zeta potential

The typical Zeta potentials observed in our analysis indicate positive surface charges, which can be attributed to the deprotonation of hydroxyl groups present on the surface of the composite material [45, 46]. The presence of hydroxyl groups plays a crucial role in influencing the surface charge properties of the material. These groups undergo deprotonation in aqueous solutions, resulting in the generation of positively charged sites on the material surface. The hydroxyl groups serve dual functions in the composite material. Firstly, they contribute to the enhancement of dispersibility by imparting a hydrophilic (polar) nature to the particles. The presence of hydrophilic groups promotes effective dispersion of the particles in aqueous media, preventing agglomeration and facilitating homogeneous distribution [47]. This improved dispersibility is crucial for various applications, including catalysis, where the accessibility of active sites is essential for reaction efficiency. Secondly, the hydroxyl groups contribute to increased electrostatic attraction between the particles. The positively charged surface sites generated by the deprotonation of hydroxyl groups promote electrostatic interactions with negatively charged species in the surrounding medium. This leads to enhanced stability of the colloidal system, as electrostatic repulsion between particles is minimized, preventing aggregation and sedimentation. Average particle size of ferrite-WFS particles was approximately distributed in the range of 761 nm [48].

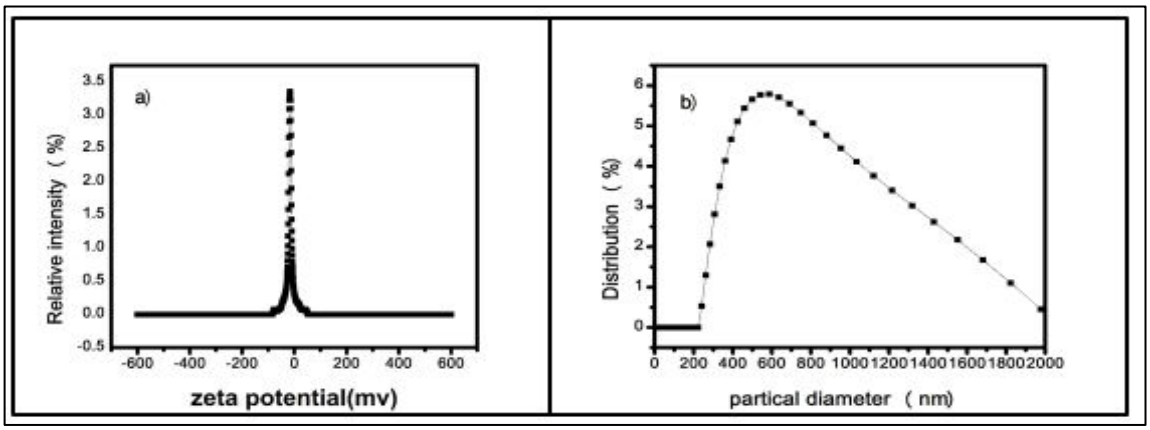

Figure.6. (a) Zeta potential (b) Particle size of WFS-Fe_3O_4

3.7. Surface area study

The determination of surface area is a crucial aspect of characterizing adsorbent materials, as it directly influences their adsorption capacity and efficiency. In our study, we employed nitrogen adsorption-desorption analysis, utilizing the Brunauer-Emmett-Teller (BET) technique, to investigate the surface area properties of the WFS-Fe_3O_4 composite. The specific surface area, pore volume, and average pore size radius of the composite were determined through the BET analysis. The specific surface area of the WFS-Fe_3O_4 composite was calculated to be 23.3268 m^2/gm. This parameter reflects the total surface area available for adsorption and interaction with adsorbate molecules, providing valuable information about the material's adsorption capacity and efficiency. The pore volume measurement indicates the total volume of pores within the material, which influences its capacity to accommodate adsorbate molecules. The average pore size radius provides insights into the size distribution of pores, affecting the accessibility of adsorbate molecules to the internal surface area of the material.

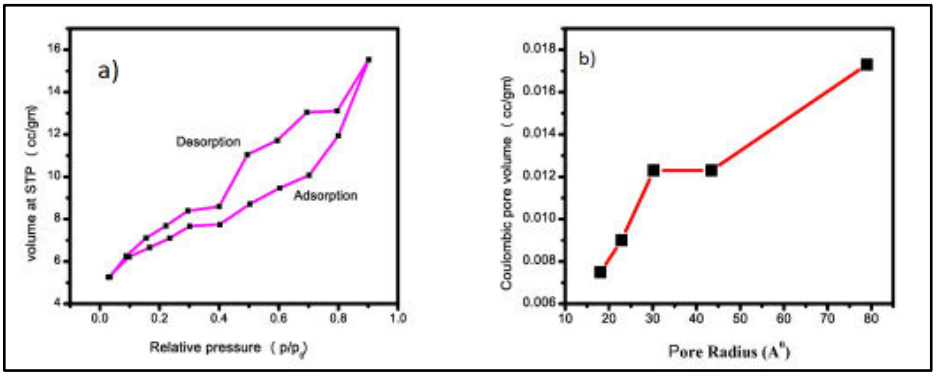

Fig.7. Brunauer-Emmett-Teller (BET) surface area of WFS-Fe_3O_4, composites

3.8. Parameters affecting photodegradation of MB

3.8.1. Effect of irradiation time

The photodegradation of methylene blue (MB) exhibits a progressive increase with extended irradiation periods, reaching after a certain duration [48, 49]. Concurrently, the absorptive intensity of MB at 664 nm shows a consistent decrease as reaction time advances. The reduction in MB dye concentration depicted in the image confirms the escalating degradation rates associated with prolonged irradiation periods [50].

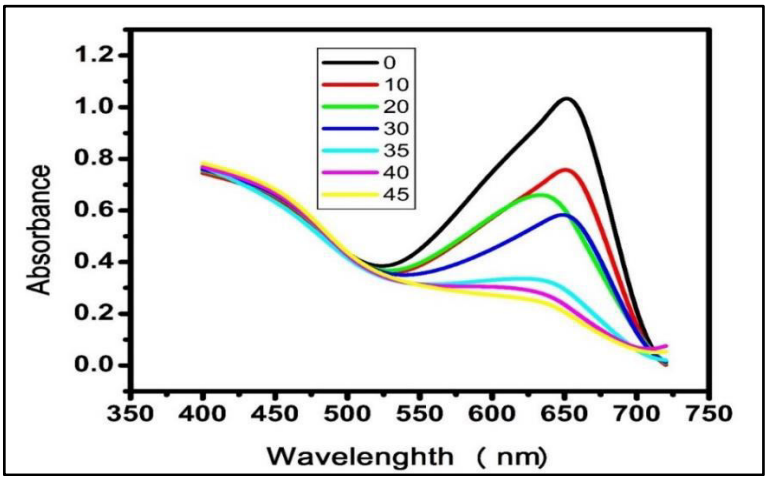

Figure.7. absorbance spectra of WFS-Fe_3O_4

3.8.2. Effect of catalyst dosage

The degradation rate was determined by introducing varying quantities of catalyst (ranging from 0.05 to 0.45 g) into a 100 mL solution containing 10 mg/L of dye at pH 8. The degradation rate exhibited a linear increase with catalyst loading up to 0.3 g, beyond which it declined. This trend can be ascribed to the escalation of turbidity and agglomeration of catalyst particles, impeding light penetration and activation [51]. Collisions between active molecules and composite ground-state molecules resulted in the deactivation of catalyst particles. Consequently, the optimal dosage of catalyst was identified to be 0.3 g [52].

3.8.3. Effect of initial dye concentration

Experiments were conducted using methylene blue (MB) dye at concentrations ranging from 10 mg/L to 40 mg/L to explore the impact of initial dye concentration on a fixed catalyst weight (0.3 g) and pH 8. The findings are presented in Fig. 8 (b). It is observed that the degradation rate of MB dye escalates at the concentration of 10 mg/L. However, due to the capping effect, the catalyst deactivates with increasing dye concentration. Consequently, there is a decline in the rate of MB degradation [53, 54].

3.8.3. Effect of pH

As the pH value varies, the surface charge of the adsorbent (catalyst) also changes. Methylene blue (MB), being a cationic dye, tends to adsorb onto a photocatalyst with a highly negative charge [55]. In basic solutions, the photocatalyst tends to acquire a negative charge due to increased electrostatic attraction, thereby enhancing the adsorption of positively charged dyes [56]. In lower pH (acidic environments), the cationic MB dye competes with H^+ ions, which are the dominant species, leading to a reduction in the ability of MB molecules to bind to the surface of the photocatalyst (Fig. 8(c))

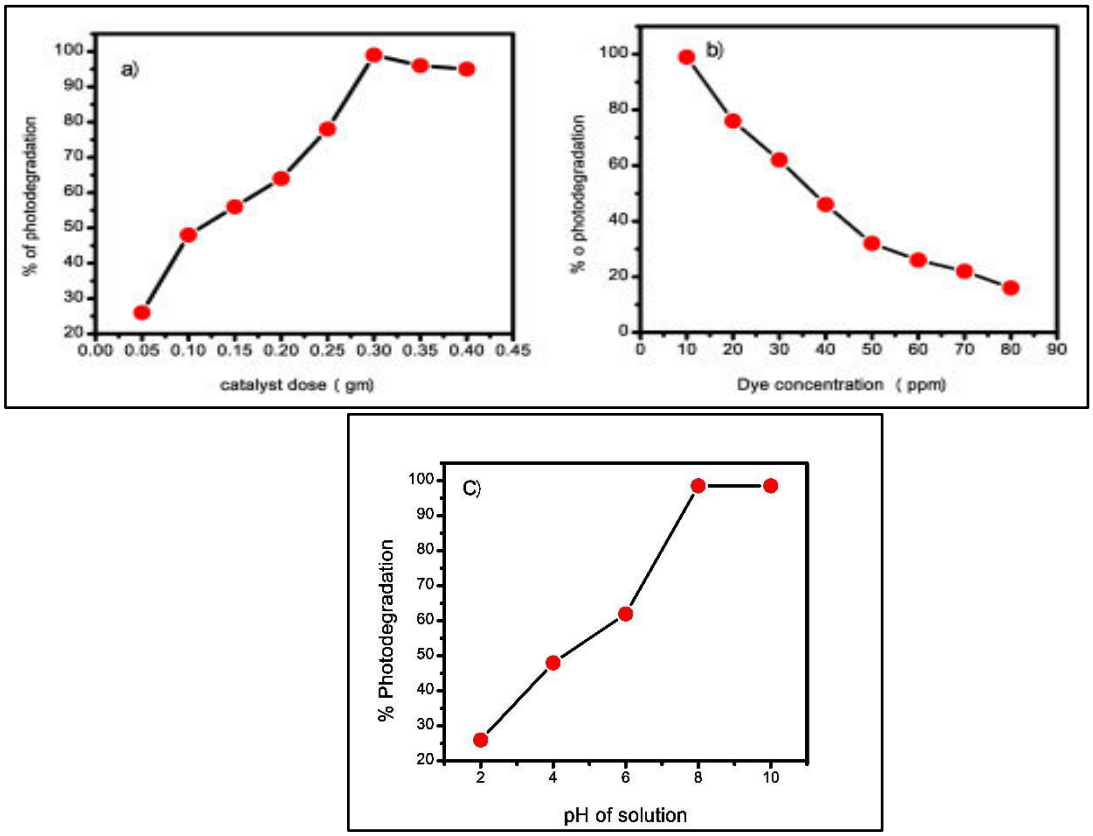

Figure.8 a) effect of catalyst dose b) effect of initial concentration c) effect of pH on degradation of MB dye.

3.9. Kinetic study of WFS-Fe_3O_4

The photodegradation of MB in the presence of WFS-Fe_3O_4 catalyst may be modelledusing the Langmuir-Hinshelwood kinetic model, which establishes a relationship between the degradation rate and the starting dye concentration [34]. Since the initial MB dye concentrations employed in this study were quite low, pseudo first-order kinetics modelling was used to analyse the data. The following formula can be used to express the kinetics:

$$C=C_0.e^{-kt} \quad \text{..... (equation 3)}$$

where ,C is the concentration of MB at time t, Co is the initial concentration of MB and k (min-1) is the degradation rate constant. The integration of Eq. 3 results in Eq. 4:

$$\ln(C/C_0) = -kt \quad \text{.....(equation 4)}$$

Based on Eq. 4, a plot of (-ln(C/Co) versus irradiation time represents a straight line showing in Fig. 5.11.

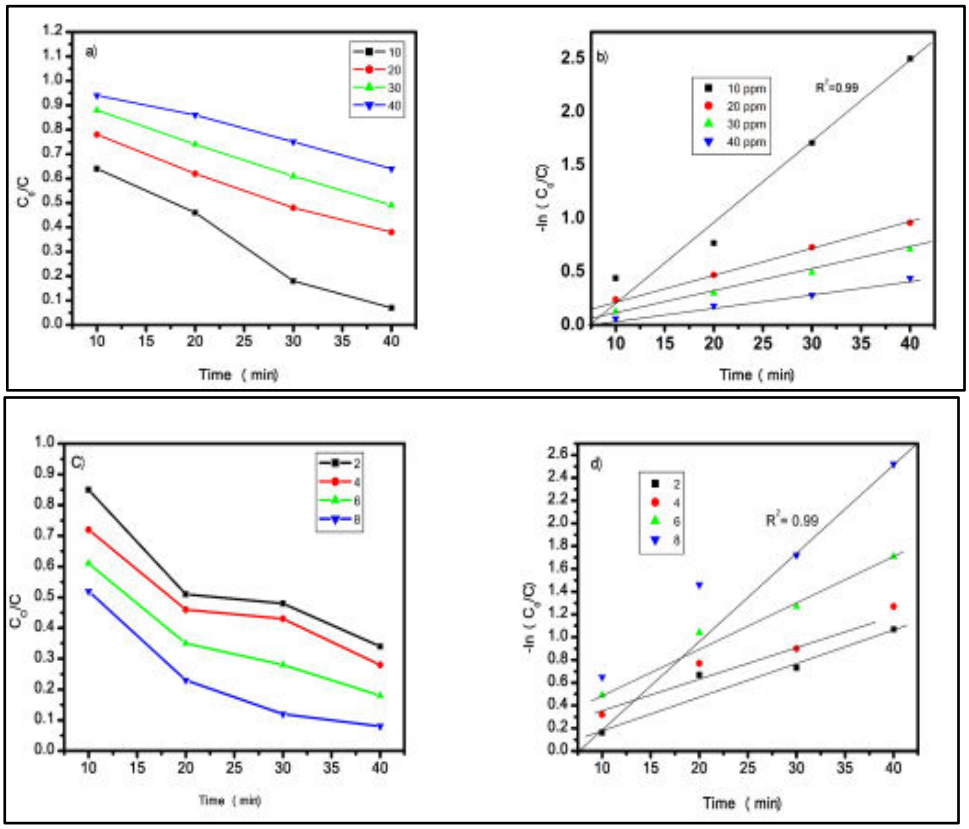

Fig. 5.11.Kinetic graph of WFS-Fe_3O_4 (a), (b) effect of concentration (c), (d) effect of pH

The value of MB degradation rate constant at each pH was shown in Table 1. From the pseudo-first-order constant, the contribution of adsorption and oxidation in the photodegradation of MB could be estimated by the equation of Langmuir-Hinshelwood model [35, 36].

Table 1.kinetic data of WFS-Fe3O4

pH	R^2	K(min^{-1})
2	0.94	1.35
4	0.96	0.01531
6	0.98	0.01357
8	0.99	0.00154

3.9.1. Recycle study of catalyst

The reusability of the WFS-Fe_3O_4 composite was evaluated through four performance cycle tests. Following each photocatalytic test, the material underwent isolation, washing with distilled water, filtration, and drying. Additionally, stability tests were conducted to evaluate the material's ability to withstand prolonged use across multiple photocatalytic cycles.

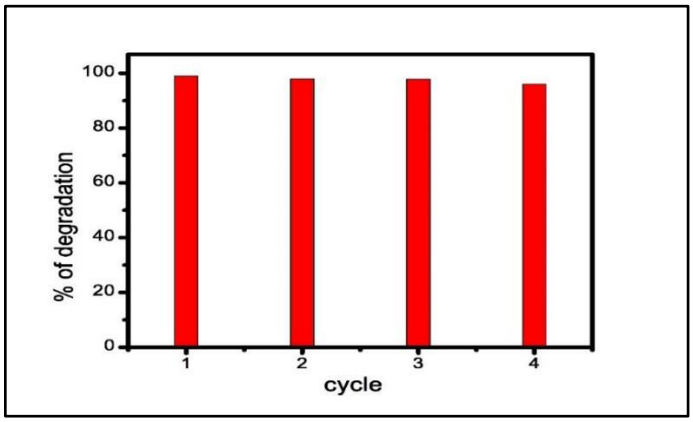

Figure. 9. Recyclability test of WFS-Fe_3O_4

4. Conclusion

In this study, we successfully synthesized WFS-Fe_3O_4 composite using the co-precipitation method. The synthesized composite exhibited several favorable characteristics, including a relatively narrow band gap energy, small crystallite size, and high surface area. Through extensive experimentation, we determined that the photocatalytic activity of the WFS-Fe_3O_4 composite yielded optimal results in degrading methylene blue (MB) dye under specific reaction conditions. These conditions included a pH of 8, a catalyst dosage of 0.3g, and an initial dye concentration of 10 mg/L. Based on the aforementioned findings, we conclude that the WFS-Fe_3O_4 composite holds promise as a highly effective material for mitigating water pollution caused by organic dyes. Its superior photocatalytic performance, coupled with its favorable characteristics, underscores its potential as a valuable tool in environmental remediation efforts.

Conflicts of Interest

The authors declare that they have no conflict of interest.

References.

1. Briffa, J., Sinagra, E., & Blundell, R. (2020). Heavy metal pollution in the environment and their toxicological effects on humans. In *Heliyon* (Vol. 6, Issue 9). Elsevier Ltd. https://doi.org/10.1016/j.heliyon.2020.e04691
2. Naidu, R., Biswas, B., Willett, I. R., Cribb, J., Kumar Singh, B., Paul Nathanail, C., Coulon, F., Semple, K. T., Jones, K. C., Barclay, A., & John Aitken, R. (2021). Chemical pollution: A growing peril and potential catastrophic risk to humanity. In *Environment International* (Vol. 156). Elsevier Ltd. https://doi.org/10.1016/j.envint.2021.106616
3. Kumari, H., Sonia, Suman, Ranga, R., Chahal, S., Devi, S., Sharma, S., Kumar, S., Kumar, P., Kumar, S., Kumar, A., & Parmar, R. (2023). A Review on Photocatalysis Used For Wastewater Treatment: Dye Degradation. In *Water, Air, and Soil Pollution* (Vol. 234, Issue 6). Institute for Ionics. https://doi.org/10.1007/s11270-023-06359-9
4. Yaqoob, A. A., Parveen, T., Umar, K., & Ibrahim, M. N. M. (2020). Role of nanomaterials in the treatment of wastewater: A review. In *Water (Switzerland)* (Vol. 12, Issue 2). MDPI AG. https://doi.org/10.3390/w12020495
5. Quddus, F., Shah, A., Iftikhar, F. J., Shah, N. S., & Haleem, A. (2023). Environmentally Benign Nanoparticles for the Photocatalytic Degradation of Pharmaceutical Drugs. In *Catalysts* (Vol. 13, Issue 3). MDPI. https://doi.org/10.3390/catal13030511
6. Fanourakis, S. K., Peña-Bahamonde, J., Bandara, P. C., & Rodrigues, D. F. (2020). Nano-based adsorbent and photocatalyst use for pharmaceutical contaminant removal during indirect potable

water reuse. In *npj Clean Water* (Vol. 3, Issue 1). Nature Research. https://doi.org/10.1038/s41545-019-0048-8

8.Wu, H., Wu, Q., Zhang, J., Gu, Q., Guo, W., Rong, S., Zhang, Y., Wei, X., Wei, L., Sun, M., Li, A., & Jing, X. (2021). Highly efficient removal of Sb(V) from water by franklinite-containing nano-FeZn composites. *Scientific Reports*, *11*(1). https://doi.org/10.1038/s41598-021-95520-7

10.Ruan, W., Hu, J., Qi, J., Hou, Y., Zhou, C., & Wei, X. (2019). Removal of dyes from wastewater by nanomaterials : A review. *Advanced Materials Letters*, *10*(1), 9–20. https://doi.org/10.5185/amlett.2019.2148

11.Bano, K., Mittal, S. K., Singh, P. P., & Kaushal, S. (2021). Sunlight driven photocatalytic degradation of organic pollutants using a MnV_2O_6/$BiVO_4$heterojunction: mechanistic perception and degradation pathways. *Nanoscale Advances*, *3*(22), 6446–6458. https://doi.org/10.1039/d1na00499a

12.Bradu, P., Biswas, A., Nair, C., Sreevalsakumar, S., Patil, M., Kannampuzha, S., Mukherjee, A. G., Wanjari, U. R., Renu, K., Vellingiri, B., & Gopalakrishnan, A. V. (2023). Recent advances in green technology and Industrial Revolution 4.0 for a sustainable future. *Environmental Science and Pollution Research*, *30*(60), 124488–124519. https://doi.org/10.1007/s11356-022-20024-4

13.Rasalingam, S., Peng, R., &Koodali, R. T. (2014). Removal of hazardous pollutants from wastewaters: Applications of TiO_2-SiO_2 mixed oxide materials. In *Journal of Nanomaterials* (Vol. 2014). Hindawi Publishing Corporation. https://doi.org/10.1155/2014/617405

15.Urso, M., Ussia, M., &Pumera, M. (2023). Smart micro- and nanorobots for water purification. *Nature Reviews Bioengineering*, *1*(4), 236–251. https://doi.org/10.1038/s44222-023-00025-9

17.Samir, A., Ashour, F. H., Hakim, A. A. A., &Bassyouni, M. (2022). Recent advances in biodegradable polymers for sustainable applications. In *npj Materials Degradation* (Vol. 6, Issue 1). Nature Publishing Group. https://doi.org/10.1038/s41529-022-00277-7

18.Vaiano, V., & de Marco, I. (2023). Removal of Azo Dyes from Wastewater through Heterogeneous Photocatalysis and Supercritical Water Oxidation. In *Separations* (Vol. 10, Issue 4). MDPI. https://doi.org/10.3390/separations10040230

19.Naseem, T., & Durrani, T. (2021). The role of some important metal oxide nanoparticles for wastewater and antibacterial applications: A review. In *Environmental Chemistry and Ecotoxicology* (Vol. 3, pp. 59–75). KeAi Communications Co. https://doi.org/10.1016/j.enceco.2020.12.001

22.Stylianou, S. K., Szymanska, K., Katsoyiannis, I. A., &Zouboulis, A. I. (2015). Novel water treatment processes based on hybrid membrane-ozonation systems: A novel ceramic membrane contactor for bubbleless ozonation of emerging micropollutants. *Journal of Chemistry*, *2015*. https://doi.org/10.1155/2015/214927

23.Avtar, R., Sahu, N., Aggarwal, A. K., Chakraborty, S., Kharrazi, A., Yunus, A. P., Dou, J., & Kurniawan, T. A. (2019). Exploring renewable energy resources using remote sensing and GIS-A review. In *Resources* (Vol. 8, Issue 3). MDPI AG. https://doi.org/10.3390/resources8030149

26.Navidpour, A. H., Abbasi, S., Li, D., Mojiri, A., & Zhou, J. L. (2023). Investigation of Advanced Oxidation Process in the Presence of TiO_2 Semiconductor as Photocatalyst: Property, Principle, Kinetic Analysis, and Photocatalytic Activity. In *Catalysts* (Vol. 13, Issue 2). MDPI. https://doi.org/10.3390/catal13020232

27.McCormick, W. J., Rice, C., McCrudden, D., Skillen, N., & Robertson, P. K. J. (2023). Enhanced Monitoring of Photocatalytic Reactive Oxygen Species: Using Electrochemistry for Rapid

Sensing of Hydroxyl Radicals Formed during the Degradation of Coumarin. *Journal of Physical Chemistry A*, *127*(23), 5039–5047. https://doi.org/10.1021/acs.jpca.3c00741

28.Khoshnam, M., Farahbakhsh, J., Zargar, M., Mohammad, A. W., Benamor, A., Ang, W. L., & Mahmoudi, E. (2021). A-Fe_2O_3/graphene oxide powder and thin film nanocomposites as peculiar photocatalysts for dye removal from wastewater. *Scientific Reports*, *11*(1). https://doi.org/10.1038/s41598-021-99849-x

29.Mayani, S. v., Bhatt, S. P., Mayani, V. J., & Sanghvi, G. (2023). Development of sustainable strontium ferrite graphene nanocomposite for highly effective catalysis and antimicrobial activity. *Scientific Reports*, *13*(1). https://doi.org/10.1038/s41598-023-33901-w

31.Kumar, H., Singh, J. P., Srivastava, R. C., Negi, P., Agrawal, H. M., & Asokan, K. (2014). FTIR and Electrical Study of Dysprosium Doped Cobalt Ferrite Nanoparticles. Journal of Nanoscience, 2014, 1–10. https://doi.org/10.1155/2014/862415.

32.Venkataraju, C., &Paulsingh, R. (2014). FTIR and EPR Studies of Nickel Substituted Nanostructured Mn Zn Ferrite. Journal of Nanoscience, 2014, 1–5. https://doi.org/10.1155/2014/815385

33.Mourdikoudis, S., Pallares, R. M., & Thanh, N. T. K. (2018). Characterization techniques for nanoparticles: Comparison and complementarity upon studying nanoparticle properties. In Nanoscale (Vol.10, Issue27, pp.12871–12934).Royal Society of Chemistry. https://doi.org/10.1039/c8nr02278j

34.Heinz, H., Pramanik, C., Heinz, O., Ding, Y., Mishra, R. K., Marchon, D., Flatt, R. J., Estrela-Lopis, I., Llop, J., Moya, S., & Ziolo, R. F. (2017). Nanoparticle decoration with surfactants: Molecular interactions, assembly, and applications. In Surface Science Reports (Vol. 72, Issue 1, pp. 1–58). Elsevier B.V. https://doi.org/10.1016/j.surfrep.2017.02.001

35.Albini, B., Restelli, S., Ambrosetti, M., Bini, M., D'Amico, F., Mozzati, M. C., &Galinetto, P. (2023). Raman spectroscopy in pure and doped zinc ferrites nanoparticles. Journal of Materials Science: Materials in Electronics, 34(12). https://doi.org/10.1007/s10854-023-10464-0

36.Ansari, S. M., Ghosh, K. C., Devan, R. S., Sen, D., Sastry, P. U., Kolekar, Y. D., & Ramana, C. v. (2020). Eco-Friendly Synthesis, Crystal Chemistry, and Magnetic Properties of Manganese-Substituted $CoFe_2O_4$Nanoparticles. ACS Omega, 5(31), 19315–19330. https://doi.org/10.1021/acsomega.9b02492

37.Guragain, D., Rai, B. K., Yoon, S., Poudel, T. P., Bhandari, S. C., & Mishra, S. R. (2020). Effect of terbium ion substitution in inverse spinel nickel ferrite: Structural and magnetic study. Magnetochemistry, 6(1), 1–9. https://doi.org/10.3390/magnetochemistry6010014

38.Cherpin, C., Lister, D., Dacquait, F., & Liu, L. (2021). Study of the solid-state synthesis of nickel ferrite ($NiFe_2O_4$) by X-ray diffraction (XRD), scanning electron microscopy (SEM) and raman spectroscopy. Materials, 14(10). https://doi.org/10.3390/ma14102557

39.Sangu, V., Kannan, K., & Srinivasan, K. (2015). Removal of mercury (II) ion from the aqueous solution using a synthetic terpolymer. In Indian Journal of Chemical Technology (Vol. 22).

40.Cherpin, C., Lister, D., Dacquait, F., & Liu, L. (2021). Study of the solid-state synthesis of nickel ferrite ($NiFe_2O_4$) by X-ray diffraction (XRD), scanning electron microscopy (SEM) and raman spectroscopy. Materials, 14(10). https://doi.org/10.3390/ma14102557

41.Nosheen, S., Iqbal, S. S., Sabir, A., Alturki, A., Hossain, N., & Bahadar, A. (2023). Synthesis and Characterizations of Novel Spinel Ferrites Nanocomposites Al0.5Cr0.5Zn0Fe_2O_4 and Zn0.5Cr0.5Al0Fe2O4. Journal of Cluster Science, 34(2), 1099–1104. https://doi.org/10.1007/s10876-022-02285-8

42.Jalaiah, K., Vijaya Babu, K., Rajashekhar Babu, K., & Chandra Mouli, K. (2018). Structural and dielectric studies of Zr and Co co-substituted $Ni0.5Zn0.5Fe_2O_4$ using sol-gel auto combustion method. Results in Physics, 9, 1417-1424. https://doi.org/10.1016/j.rinp.2018.04.024

43.Jalaiah, K., Chandra Mouli, K., Vijaya Babu, K., & Krishnaiah, R. v. (2019). Structural, electrical and magnetic properties of Mg-Zr co-substituted $Ni0.5Zn0.5Fe_2O_4$. Journal of Science: Advanced Materials and Devices, 4(2), 310-318. https://doi.org/10.1016/j.jsamd.2018.12.004

44.Zorai, A., Souici, A., Dragoe, D., Rivière, E., Ouhenia, S., Belloni, J., & Mostafavi, M. (2022). Superparamagnetic cobalt ferrite nanoparticles synthesized by gamma irradiation. New Journal of Chemistry, 47(5), 2626-2634. https://doi.org/10.1039/d2nj05433g.

45.Naaz, F., Dubey, H. K., Kumari, C., & Lahiri, P. (2020). Structural and magnetic properties of MgFe2O4 nanopowder synthesized via co-precipitation route. SN Applied Sciences, 2(5). https://doi.org/10.1007/s42452-020-2611-9

46.Hasan, S., &Azhdar, B. (2022). Synthesis of Nickel-Zinc Ferrite Nanoparticles by the Sol-Gel Auto-Combustion Method: Study of Crystal Structural, Cation Distribution, and Magnetic Properties. Advances in Condensed Matter Physics, 2022. https://doi.org/10.1155/2022/4603855

47.Hasan, S., &Azhdar, B. (2022). Synthesis of Nickel-Zinc Ferrite Nanoparticles by the Sol-Gel Auto-Combustion Method: Study of Crystal Structural, Cation Distribution, and Magnetic Properties. Advances in Condensed Matter Physics, 2022. https://doi.org/10.1155/2022/4603855.

48.Vavilapalli, D.S.; Peri, R.G.; Sharma, R.K.; Goutam (2021), U.K.; Muthuraaman, B.; Ramachandra Rao, M.S.; Singh, S. g-C3N4/$Ca_2Fe_2O_5$ heterostructures for enhanced photocatalytic degradation of organic effluents under sunlight. Sci. Rep., 11, 19639.

49. Saleh, R.; Taufik, A. (2019,) Photo-Fenton degradation of methylene blue in the presence of Au-Fe_3O_4/graphene composites under UV and visible light at near neutral pH: Effect of coexisting inorganic anion. Environ. Nanotechnol. Monit. Manag. 11, 100221.

50. Pan, X.; Cheng, S.; Su, T.; Zuo, G.; Zhao, W.; Qi, X.; Wei, W.; Dong, W. (2019) Fenton-like catalyst Fe_3O_4@polydopamine-MnO_2 for enhancing removal of methylene blue in wastewater. Colloids Surf. B Biointerfaces, 181, 226-233.

51. Sharma, C.P.; Karim, A.V.; Shriwastav, A. (2019) Decolorization of methylene blue using Fe(III)-citrate complex in a solar photo-Fenton process: Impact of solar variability on process optimization. Water Sci. Technol., 80, 2047-2057.

52. Alkaim, A.F.; Aljeboree, A.M.; Alrazaq, N.A.; Baqir, S.J.; Hussein, F.H.; Lilo, A.J. (2014), Effect of pH on adsorption and photocatalytic degradation efficiency of different catalysts on removal of methylene blue. Asian J. Chem. 26, 8445-8448.

53. Anju Chanu, L.; JoychandraSingh,W.; Jugeshwar Singh, K.; Nomita Devi, K. (**2019**) Effect of operational parameters on the photocatalytic degradation of Methylene blue dye solution using manganese doped ZnO nanoparticles. Results Phys., 12, 1230-1237

54. Enesca, A.; Isac, L. **(2020)** The Influence of Light Irradiation on the Photocatalytic Degradation of Organic Pollutants.Materials.

55. Nuengmatcha, P.; Porrawatkul, P.; Chanthai, S.; Sricharoen, P.; Limchoowong, N. (2019)Enhanced photocatalytic degradation of methylene blue using Fe_2O_3/graphene/CuOnanocomposites under visible light. J. Environ. Chem. Eng., 7, 103438.

56. Balu, S.; Uma, K.; Pan, G.T.; Yang, T.C.K.; Ramaraj, S.K. (2018) Degradation of methylene blue dye in the presence of visible light using SiO_2@_-Fe_2O_3 nanocomposites deposited on SnS_2 flowers. Materials, 11, 1030.